Title

Improved subseasonal-to-seasonal precipitation prediction of climate models with nudging approach for better initialization of Tibetan Plateau-Rocky Mountain Circumglobal wave train and land surface conditions

Authors

Qin, Yi
Tang, Qi
Xue, Yongkang
et al.

Publication Date

2024

DOI

10.1007/s00382-023-07082-1

Peer reviewed

Climate Dynamics
https://doi.org/10.1007/s00382-023-07082-1

ORIGINAL ARTICLE

Improved subseasonal-to-seasonal precipitation prediction of climate models with nudging approach for better initialization of Tibetan Plateau-Rocky Mountain Circumglobal wave train and land surface conditions

Yi Qin[1,2] · Qi Tang[1] · Yongkang Xue[3] · Ye Liu[2] · Yanluan Lin[4]

Received: 3 May 2023 / Accepted: 21 December 2023

Abstract
Reliable subseasonal-to-seasonal (S2S) precipitation prediction is highly desired due to the great socioeconomical implications, yet it remains one of the most challenging topics in the weather/climate prediction research area. As part of the Impact of Initialized Land Temperature and Snowpack on Sub-seasonal to Seasonal Prediction (LS4P) project of the Global Energy and Water Exchanges (GEWEX) program, twenty-one climate models follow the LS4P protocol to quantify the impact of the Tibetan Plateau (TP) land surface temperature/subsurface temperature (LST/SUBT) springtime anomalies on the global summertime precipitation. We find that nudging towards reanalysis winds is crucial for climate models to generate atmosphere and land surface initial conditions close to observations, which is necessary for meaningful S2S applications. Simulations with nudged initial conditions can better capture the summer precipitation responses to the imposed TP LST/SUBT spring anomalies at hotspot regions all over the world. Further analyses show that the enhanced S2S prediction skill is largely attributable to the substantially improved initialization of the Tibetan Plateau-Rocky Mountain Circumglobal (TRC) wave train pattern in the atmosphere. This study highlights the important role that initial condition plays in the S2S prediction and suggests that data assimilation technique (e.g., nudging) should be adopted to initialize climate models to improve their S2S prediction.

Keywords Nudging · Initialization method · S2S prediction · Tibetan Plateau-Rocky Mountain Circumglobal wave train · Climate model · Tibetan Plateau

1 Introduction

The Impact of Initialized Land Surface Temperature and Snowpack on Subseasonal to Seasonal Prediction (LS4P) project of the Global Energy and Water Exchanges (GEWEX) program aims to study the impact of springtime land surface temperature (LST)/subsurface temperature (SUBT) anomalies over high mountain areas on summertime precipitation prediction locally and remotely, and to improve process understanding of the driving mechanism (Xue et al. 2021, 2022). During LS4P Phase I, 21 climate models participated in simulating the precipitation response in June 2003 to LST/SUBT anomalies over the Tibetan Plateau (TP) in May 2003. However, many climate models failed to reproduce the observed anomalies in terms of locations and magnitudes with Atmospheric Model Intercomparison Project (AMIP-type) (Gates et al. 1999) simulations (Xue et al. 2021). This is because climate models are mainly designed for long-term (decades to centuries) climate research, emphasizing mean climatology, variability, and future climate change (Arias et al. 2021). Applying climate models for subseasonal-to-seasonal (S2S) prediction is beyond their primary scientific objective and naturally face difficulties due to inherent limitations, including but not limited to lack

✉ Qi Tang
tang30@llnl.gov

1 Lawrence Livermore National Laboratory, Livermore, CA, USA

2 Pacific Northwest National Laboratory, Richland, WA, USA

3 Department of Geography, University of California Los Angeles, Los Angeles, CA, USA

4 Department of Earth System Science, Tsinghua University, Beijing, China

Published online: 03 February 2024

of good initial conditions (Mariotti et al. 2018; Xue et al. 2021) and the unresolved physical processes with standard climate resolution (~ 100 km). A specific time (e.g., day, month) in AMIP-type climate simulations does not represent the actual one in the observation and the discrepancy arises due to factors such as model initialization, parameterizations, forcing data accuracy, and natural variability. Therefore, climate models generally are not used in S2S studies that specifically aim to match time-specific observations. In particular, large discrepancies in the initial atmosphere and land conditions of climate models relative to observations could be one potential issue.

The nudging approach, a simple data assimilation method, has been used to adjust the model state variables to observational or reanalysis data. It has been proven to be effective for generating more accurate initial conditions in climate models. Such method is adopted in climate simulations for two main purposes: (1) it increases the signal-to-noise ratio for sensitivity experiments to better isolate and understand the impact of specific factors on the climate system (Sun et al. 2019; Tang et al. 2019; Zhang et al. 2014); and (2) it can be used to evaluate the model results with observations under constrained atmospheric conditions as in the hindcast studies (Jeuken et al. 1996; Phillips et al. 2004; Xie et al. 2012; Ma et al. 2015).

Land initialization and configuration have been identified as one of the major avenues for improving S2S prediction (Merryfield et al. 2020). Considering the substantially greater impact of initial conditions on the S2S scale than on the climate scale, we hypothesize that better land initial conditions are necessary for successful LS4P S2S simulations using climate models. Furthermore, a recent study (Xue et al. 2022) revealed the importance of the large-scale pattern (i.e., Tibetan Plateau-Rocky Mountain Circumglobal (TRC) wave train) in producing adequate response to the imposed TP LST/SUBT anomalies for a successful S2S global precipitation prediction. Thus, we also examine the impact of the better initialization of the large-scale wave train due to nudging on the global S2S precipitation prediction.

In this study, we investigate the impact of the nudging approach on the LS4P simulations using two climate models: the Department of Energy (DOE) Energy Exascale Earth System Model (E3SM) version 1 (Golaz et al. 2019; Rasch et al. 2019) and Community Integrated Earth System Model (CIESM) (Lin et al. 2020). The selection of the two models is based on their respective warm (CIESM) and cold (E3SMv1) biases in surface air temperature compared to the observation over the TP, which represent two groups of LS4P climate models that share similar biases (Xue et al. 2021). The remaining sections are arranged as follows. We briefly introduce the two models and the nudging approach in Sect. 2. Section 3 presents the impact of the nudging approach on atmosphere and land initial conditions and global summertime precipitation response to the imposed TP LST/SUBT anomalies, followed by conclusions and discussions in Sect. 4.

2 Method

2.1 Model description

The Energy Exascale Earth System Model (E3SM) version 1 (E3SMv1; Golaz et al. 2019; Rasch et al. 2019) and Community Integrated Earth System Model (CIESM) (Lin et al. 2020) are both fully coupled climate models, including atmosphere, ocean, sea ice, land, and river transport components. Following the LS4P protocol (Xue et al. 2021), we perform the AMIP-type experiments with prescribed sea surface temperature (SST) and sea ice from observations. Since the atmosphere and land models are active in AMIP-type experiments, we briefly summarize the atmospheric and land schemes used in these two models in Table 1 and describe their differences below.

The two models are similar in many aspects. Both run with the spectral element dynamical core (Dennis et al. 2012), with around ~ 100 km horizontal resolution and 72 vertical levels with a top at approximately 60 km in E3SMv1 and 30 vertical levels with a top at approximately 40 km in CIESM. They share some common parameterizations, including the Zhang-McFarlane (ZM) deep convection parameterization (Zhang and McFarlane 1995), the Rapid Radiative Transfer Model for GCMs (RRTMG) (Iacono et al. 2008), and the Morrison and Gettelman (MG) cloud microphysics scheme but with different modifications. CIESM includes stochasticity and convective microphysics (Song and Zhang 2011; Wang et al. 2016) in ZM deep convection scheme. E3SMv1 uses the default two-stream shortwave radiation scheme and CIESM uses a four-stream shortwave radiation (Zhang and Li 2013) in RRTMG. E3SMv1 uses MG version 2 (Gettelman and Morrison 2015), while CIESM uses MG version 1.5 using a single ice approach (Morrison and Gettelman 2008; Zhao et al. 2017).

The two models use distinct parameterizations in other modules. E3SMv1 uses the Cloud Layers Unified by Binormals (CLUBB) (Golaz et al. 2002; Larson and Golaz 2005) which unifies the treatment of shallow convection, cloud macrophysics and turbulence. CIESM uses the University of Washington shallow convection and moist turbulence schemes (Bretherton and Park 2009; Park and Bretherton 2009) and a probability density function (PDF) based cloud macrophysics scheme (Qin et al. 2018). The sub-grid orographic form drag scheme is Turbulent Mountain Stress scheme (Neale et al. 2012) and BBW04 scheme (Beljaars et al. 2004; Liang et al. 2017) in E3SMv1 and CIESM,

Table 1 Atmospheric physical schemes and land model of E3SMv1 and CIESM

Scheme	E3SMv1	CIESM
Deep convection	Zhang-McFarlane scheme with modifications to accommodate EAM's resolution (Rasch et al. 2019)	Zhang-McFarlane scheme with stochasticity and convective microphysics (Song and Zhang 2011; Wang et al. 2016)
Cloud microphysics	MG2.0 (Gettelman and Morrison 2015)	MG1.5 with updated cloud ice scheme (Zhao et al. 2017)
Aerosol	Improved MAM4 (Liu et al. 2016)	Prescribed aerosols (Stevens et al. 2017)
Radiation	RRTMG	RRTMG with four-stream shortwave radiation (Zhang and Li 2013)
Shallow convection	CLUBB (Golaz et al. 2002; Larson and Golaz 2005)	UW shallow convection (Park and Bretherton 2009)
Cloud macrophysics	CLUBB	PDF cloud scheme (Qin et al. 2018)
Planetary boundary layer	CLUBB	UW turbulence (Bretherton and Park 2009)
Orographic form drag	Turbulent Mountain Stress scheme (Neale et al. 2012)	BBW04 scheme (Beljaars et al. 2004; Liang et al. 2017)
Land model	ELMv0 (Golaz et al. 2019)	CLM 4.0 (Oleson et al. 2010)

respectively. For aerosols, E3SMv1 uses the interactive aerosol model—Modal Aerosol Module (MAM4) (Liu et al. 2016) with some improvements, and CIESM follows the approach proposed by Coupled Model Intercomparison Project Phase 6 (Eyring et al. 2016) using the prescribed aerosol forcing dataset MACv2-SP (the second version of the Max Planck Institute Aerosol Climatology) (Stevens et al. 2017). For the two models, the bulk exchange formation is used to describe the surface exchange of heat, moisture and momentum between the atmosphere and land, ocean or ice surfaces (Neale et al. 2012). The coupling of different model components is handled by CPL7 (Larson et al. 2005; Craig et al. 2012) in E3SMv1 and Community Coupler Version 2 (C-Coupler2) (Liu et al. 2018) in CIESM. More details about model performance and other model components of these two models refer to Golaz et al. (2019) and Lin et al. (2020).

The accuracy of LST/SUBT simulation tightly relies on how surface radiation and heat fluxes are represented (Huang et al. 2020). CLM versions 4.0 and ELM version 0 (branched from CLM version 4.5) use the same basic theories for this purpose, including the two-stream approximation (Seller 1985), bulk transfer equation (Verhoef et al. 1997), and heat transfer equation for canopy radiation transfer, heat fluxes, and soil heat transfer, respectively. However, ELMv0 introduced new features including considering aerosols and black carbon on snow and adjusting leaf stomatal conductance and land albedo. These changes result in differences in energy balance calculations compared to the previous version (Golaz et al. 2019). Additionally, CLM 4.0 in CIESM incorporated new datasets for soil texture and organic matter content, which affects LST/SUBT through changing soil thermal and hydraulic properties.

The E3SMv1 and CIESM use different planetary boundary layer (PBL) schemes which can influence LST calculation via affecting turbulence, cloud processes, and land–atmosphere interactions. The UW turbulence scheme used in CIESM is specialized in modeling turbulence while the CLUBB scheme used in E3SMv1 is more comprehensive as it integrates multiple processes, including turbulence, shallow convection, and cloud macrophysics. Their different PBL closure assumptions would affect the turbulent flux, and further redistribute the temperature and moisture in PBL, which influences the surface fluxes and LST/SUBT. Additionally, compared to the separate schemes for cloud macrophysics and turbulence in CIESM, CLUBB better deals with the sub-grid interaction between cloud and turbulence. The different cloud parameterizations can also affect the incoming radiation at the surface and further affect the LST/SUBT.

2.2 Experiment setup

Following the LS4P protocol (Xue et al. 2021), each experiment consists of two simulations to investigate the impact of springtime TP LST/SUBT anomaly on summertime precipitation. Firstly, the model runs for two months starting from May 1st through June 30th, 2003 (EXP1). Because models have large biases over the TP (Xue et al. 2021), we produce a land mask over the TP based on the simulation bias of the 2-m air temperature (T2m) and observed T2m anomaly for May 2003. This land mask is used to reduce the T2m bias over the TP area. We impose this mask for all soil layers at the first time step of May 1st and re-run the model from May 1st through June 30th (EXP2). The approach to generate the mask is described in Xue et al. (2021) in detail. The difference between EXP2 and EXP1 (as listed in Table 2) denotes the impact of LST/SUBT effect.

Nudging method is a data assimilation method that uses an additional term in the model equations to drive the model towards a reference state, which can be observed data, reanalysis, or a higher resolution model result. The equation for nudging can be expressed as:

Table 2 List of the experiments for E3SMv1 and CIESM

Short name	Description	Simulation period
EXP0	Experiment **without** nudging	1 month (April 1 to April 30)
EXP0-Nudg	Experiment **with** nudging	As above for CIESM and 4 months (Jan 1 to April 30) for E3SMv1
EXP1	Experiment **without** nudged initial conditions (IC)	2 months (May 1 to June 30)
EXP2	Experiment **without** nudged IC + imposed TP anomaly	As above
EXP1-NudgIC	Experiment **with** nudged IC	As above
EXP2-NudgIC	Experiment **with** nudged IC + imposed TP anomaly	As above

$$\frac{\partial X}{\partial t} = F(X) - \frac{X - Xr}{\tau}$$

where X is the state of the model, F is the tendency caused by dynamic and physical processes. The nudging term is written as $-(X - Xr)/\tau$, where τ is the nudging relaxation time scale, and Xr is the reference state. More details about this approach can be found in Sun et al. (2019), which covers what data used to constrain the model, what variables to be nudged at which vertical levels, how large the nudging strength is and how often to apply nudging, and their impacts on simulations. In this study, we only nudge the horizontal winds at all vertical levels, which helps produce a more realistic initial condition of large-scale wave pattern, and also generate more consistent clouds and aerosol properties as observed (Ma et al. 2015; Zhang et al. 2014). The nudging is conducted at every model timestep (1800s) to European Center for Medium-range Weather Forecasting Interim (ERAI) reanalysis (Dee et al. 2011), which are available at 00Z, 06Z, 12Z and 18Z, and are linearly interpolated to each model timestep from neighboring time slices. The reanalysis data are interpolated to the model's horizontal grid following the procedures described in Boyle et al. (2005) and Xie et al. (2012), which includes adjustments to account for the different representation of topography. The relaxation time scale is 6 h following previous studies (Kooperman et al. 2012; Tang et al. 2019). The atmospheric nudging process of CIESM is illustrated in Fig. 1 as an example.

EXP0 is used to generate initial conditions for EXP1 and EXP2 without nudging. No Nudging is employed in EXP1 and EXP2. The E3SMv1 and CIESM nudging simulations (termed EXP0-Nudg) start on January 1st and April 1st, 2003, respectively, and end on April 30th, 2003 (Fig. S2). The EXP0-Nudg run on April 30th is used to initialize the subsequent EXP1-NudgIC and EXP2-NudgIC experiments. The difference between EXP2-NudgIC and EXP1-NudgIC denotes the impact of LST/SUBT effect after nudging is applied to generate the initial condition. All simulations used in this study are summarized in Table 2.

All experiments have six and eight ensemble members for E3SMv1 and CIESM, respectively. The ensemble mean is used for the later analysis. The ensembles are created by adding white noises in the temperature field of the initial condition. When creating the land temperature mask, the simulated 2-m air temperature (T2m) was adjusted with a lapse rate to account for the differences between the model's topography and the elevation of observational sites (Xue et al. 1996; Gao et al. 2017).

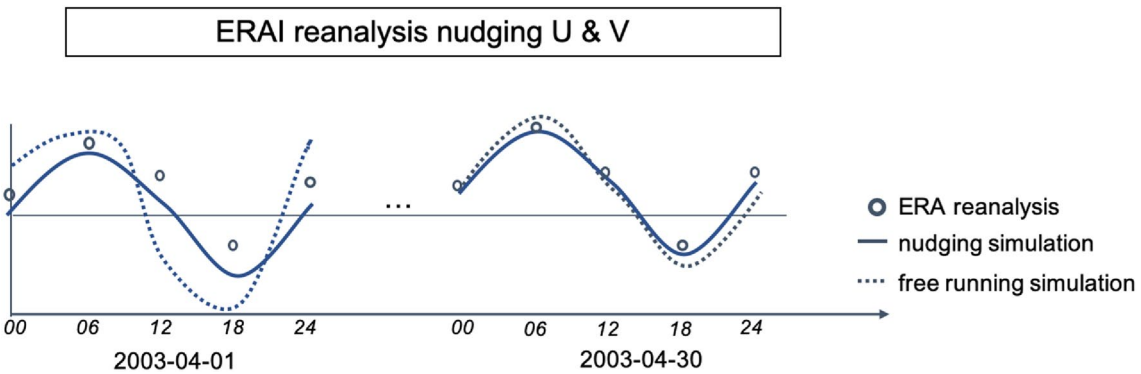

Fig. 1 Schematic of the atmospheric nudging process

2.3 Observational data

We use the composite monthly datasets for global May T2m and June precipitation (Xue and Diallo 2020) with the spatial resolution of 100 km for the year of 2003. In this dataset, the T2m and precipitation data for regions other than China were obtained from the Climate Anomaly Monitory System (CAMS) and Climate Research Unit (CRU), respectively. The Chinese Meteorological Administration (CMA) data was used for China. The composite datasets are used to quantify the model's bias and generate the land mask, which is applied to evaluate the model's ability to simulate May T2m anomaly and June precipitation response. Note that separate land masks are generated for experiments with and without nudged initial conditions.

3 Results

3.1 The impact of nudging on initial conditions

In this section, we compare EXP0 and EXP0-Nudg experiments in Table 2 to examine the impact of nudging on initial conditions. The spatial patterns of 2-m air temperature, zonal and meridional winds at 850 hPa on April 15, 2003 (Fig. 2) show better agreement with the ERAI data in EXP0-Nudg than in EXP0 of E3SMv1. These results confirm that the nudging method is effective. The spatial correlation between ERAI and E3SMv1 EXP0-Nudg and EXP0 are 0.98 and 0.50, respectively. The time-evolving global mean values get close to the ERAI value in the entire April, especially for zonal and meridional winds at 850 hPa because these two variables are directly nudged to the ERAI data. For the 2-m air temperature, EXP0 and EXP0-Nudg are not very different from the ERAI because sea surface temperature is

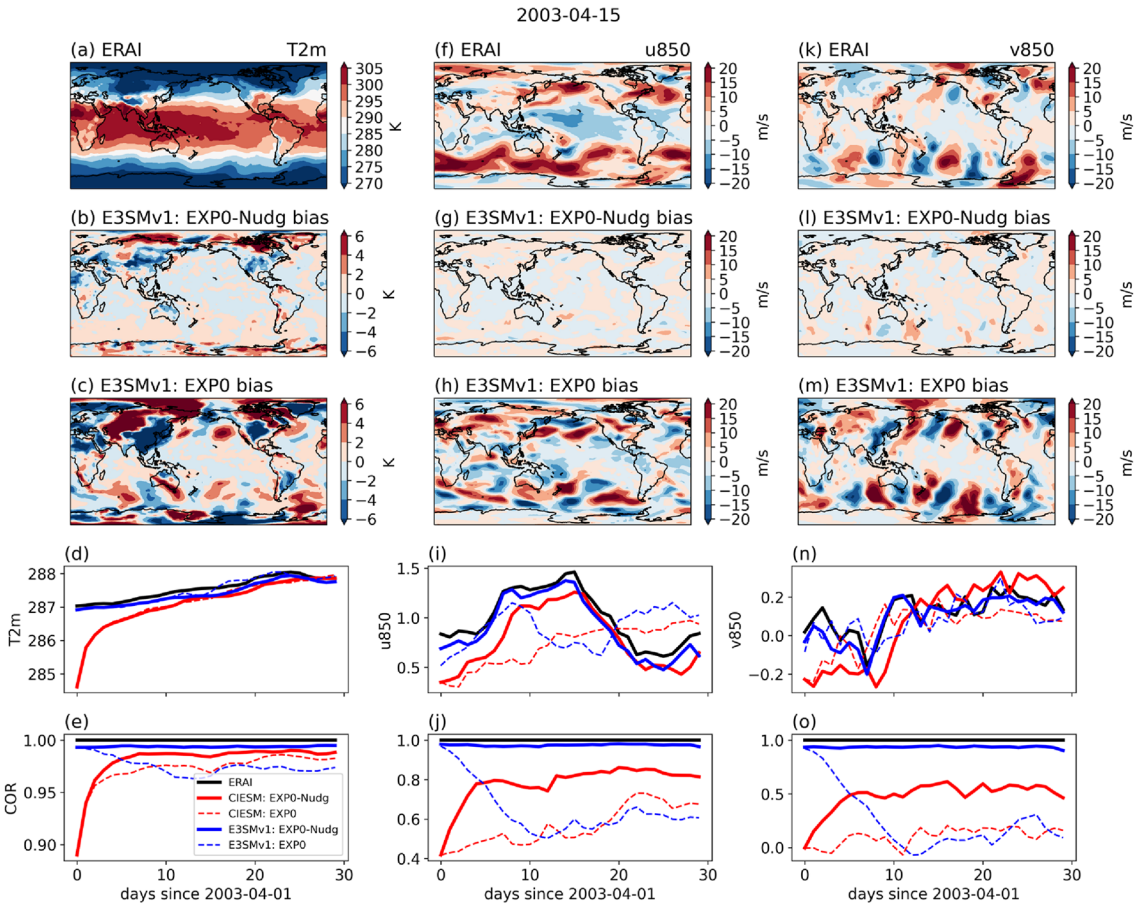

Fig. 2 Spatial maps of 2-m air temperature (T2m; K), zonal wind at 850 hPa (u850; m/s), meridional wind at 850 hPa (v850; m/s) from ERAI (**a**, **f**, **k**), the difference between E3SMv1 EXP0-Nudg and ERAI (**b**, **g**, **l**) and the difference between E3SMv1 EXP0 and ERAI (**c**, **h**, **m**) experiments on April 15, 2003. Panels (**d**, **i**, **n**) show the time-evolving global-mean values from ERAI (black solid), CIESM EXP0-Nudg (red solid), CIESM EXP0 (red dashed), E3SMv1 EXP0-Nudg (blue solid) and E3SMv1 EXP0 (blue dashed). Panels (**e**, **j**, **o**) show the time-evolving spatial correlations (COR) between each experiment and ERAI data for the three variables

prescribed with the same observation. Nevertheless, the spatial correlation of 2-m air temperature between EXP0-Nudg and the observation is slightly higher than that with EXP0 (Fig. 2e). With the nudging approach, the spatial correlation of winds at 850 hPa between the simulation and ERAI is largely improved (Fig. 2j and o), especially for E3SMv1, which has a spatial correlation of around 1.0 for all three variables. The relatively lower spatial correlation of CIESM EXP0-Nudg and ERAI than E3SMv1 EXP0-Nudg and ERAI is likely because CIESM only runs one-month with nudging while E3SMv1 nudges for four months.

We further examine the root mean square error (RMSE) of the three variables relative to ERAI and available observations for EXP0-Nudg and EXP0 averaging from April and April 30th, which is the day next to the starting date of the standard EXP1 and EXP2 experiments. EXP0-Nudg experiments overall show smaller RMSE than that from EXP0 experiments over the globe, East Asia (5° N–80° N, 40° E–180° E) and TP (26° N–39° N, 73.2° E–104.5° E) for April and April 30th (Fig. 3). We also find that the RMSE of April 2-m air temperature is decreased in EXP0-Nudg experiments when compared with the CMA-CAMS dataset (marked by unfilled triangles in Fig. 3). Therefore, we conclude that applying the nudging approach indeed improves the mean April atmospheric states and provides a more realistic atmospheric initial condition for the later standard LS4P experiments (EXP1-NudgIC and EXP2-NudgIC).

Since the scientific goal of LS4P targets on investigating the impact of TP LST/SUBT anomaly on the global surface temperature and precipitation responses, it is necessary to examine whether the nudging approach helps build a better LST/SUBT initial condition over the TP for such S2S predictions. We use the observed soil temperature from 15 sites over the TP provided by the China

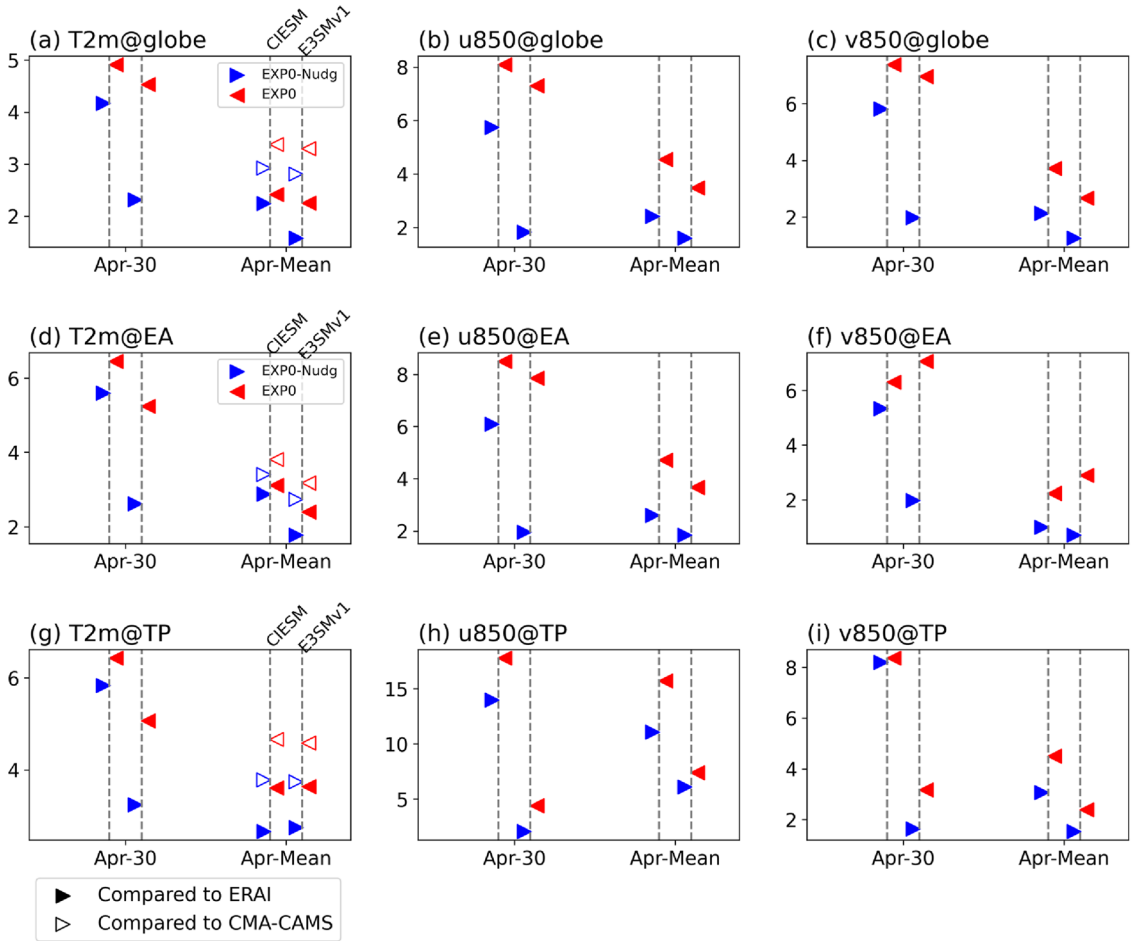

Fig. 3 Root Mean Square Error (RMSE) of 2-m air temperature (T2m; K), zonal wind at 850 hPa (u850; m/s) and meridional wind at 850 hPa (v850; m/s) between CIESM and ERAI (first vertical line) and E3SMv1 and ERAI (second vertical line) on April 30th, 2003 and monthly mean in April 2003 over the globe (**a–c**), East Asia (5° N–80° N, 40° E–180° E) (**d–f**), and TP (26° N–39° N, 73.2° E–104.5° E) (**g–i**). The red triangles denote the results from EXP0, and the blue triangles denote the results from EXP0-Nudg. The filled and unfilled triangles are, respectively, compared to ERAI and CMA-CAMS observation dataset for April 2003

Meteorological Administration (https://data.cma.cn). The locations of these sites are delineated in Fig. S1. We compare the upper layer (0–0.8 m) soil temperature from the two models with the observation (Fig. 4). The models generally produce strong cold biases of the soil temperature at all sites. Compared to the experiments without using nudging (EXP0), the experiments using nudging (EXP0-Nudg) tend to alleviate the cold bias in most sites. It is not only in LST, but also SUBT in some sites. But the improvement is relatively smaller than the atmospheric variables, which are directly nudged. The 0–7 cm soil temperature from ERAI also shows cold biases compared to the observation, but the magnitudes of the ERAI bias is weaker than that from the models at some sites (e.g., sites 51,828, 52,818, 52,602). These results suggest that both ERAI reanalysis data and the two climate models used here have deficiencies in capturing the observed soil temperature, and the sensitivity experiments with imposed LST/SUBT anomalies over the TP are crucial to understand their impacts on S2S precipitation prediction.

The model's ability to correctly simulate synoptic wave pattern is crucial to capture the impact of LST/SUBT anomaly on the remote precipitation prediction. Xue et al. (2022) indicated that those hotspots region along the Tibetan Plateau-Rocky Mountain Circumglobal (TRC) wave train show more consistencies among the LS4P climate models. This wave train starts from the TP through Northern East Asia and the Bering Strait to the western part of North America. The TP LST/SUBT influences the precipitation in the downstream region, including North America, through a midlatitude wave train signal. To examine the impact of nudging on the initial synoptic wave pattern, we evaluate the fidelity of simulated non-zonal geopotential height at 200 hPa on April 30th, 2003 (Fig. 5), which could represent the initial condition of the wave train. Overall, the experiments without using nudging (EXP0) suffer difficulties in capturing the ERAI wave pattern. For example, the EXP0 of E3SMv1 shows high-pressure anomalies over western North America and low-pressure anomalies over eastern North America, which is opposite from that in ERAI. In

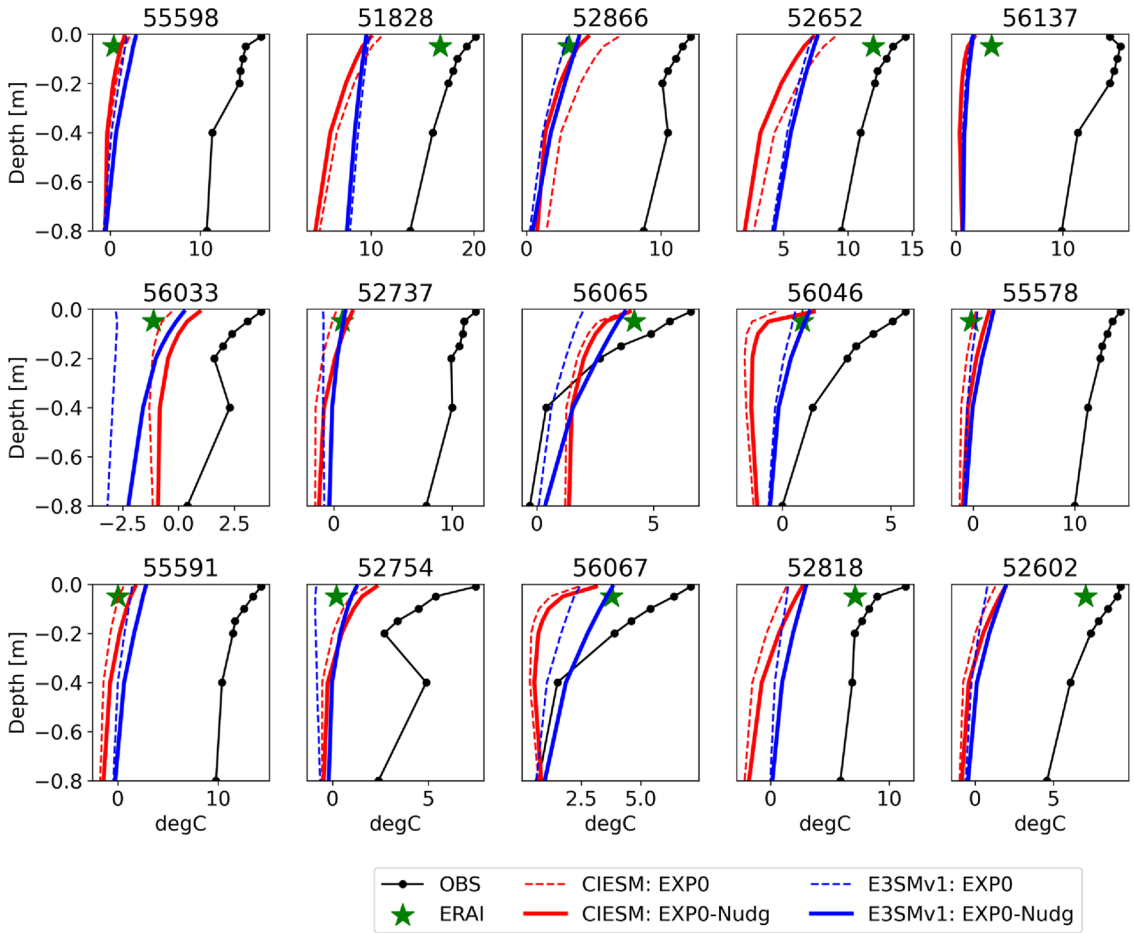

Fig. 4 Soil temperature profiles at observational sites shown in Fig. S1. Black: observation; blue dashed: E3SMv1 EXP0; red solid: E3SMv1 EXP0-Nudg; red dashed: CIESM EXP0; blue solid: CIESM EXP0-Nudg; green asterisk: ERAI

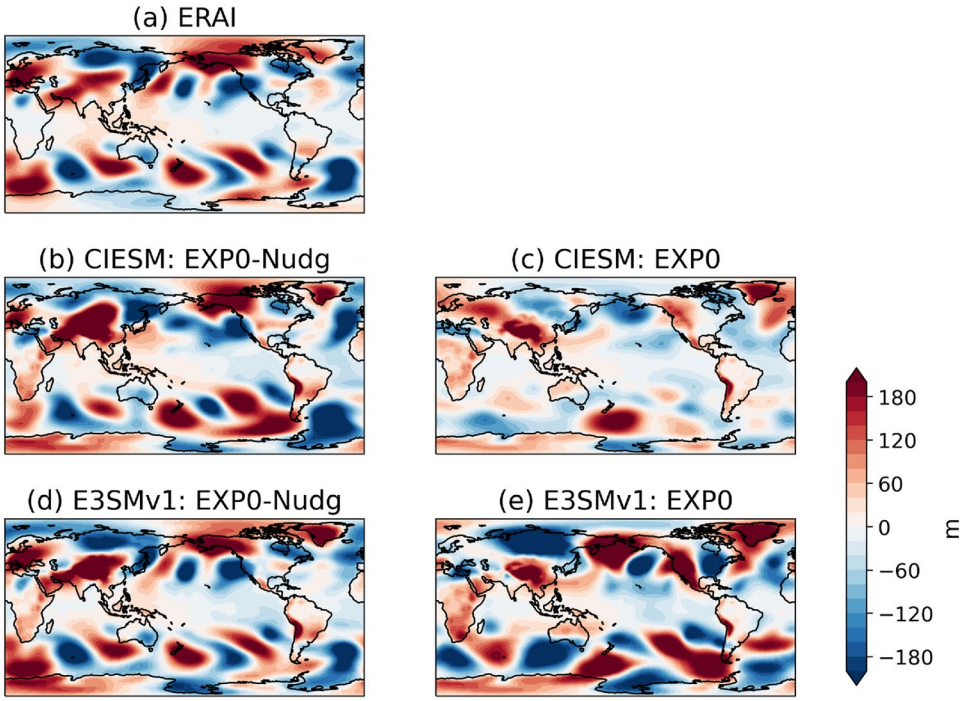

Fig. 5 Non-zonal geopotential height at 200 hPa (m) from **a** ERAI, **b** CIESM EXP0-Nudg, **c** CIESM EXP0, **d** E3SMv1 EXP0-Nudg, and **e** E3SMv1 EXP0 on April 30th, 2003

general, the simulations using nudging (EXP0-Nudg) from both models improve the simulated wave train pattern over their counterpart without using nudging (EXP0). Therefore, nudging provides a good atmospheric large-scale condition for simulating the impact of TP LST/SUBT anomaly on precipitation prediction through teleconnections.

In summary, we establish that the nudging approach indeed helps generate a better atmospheric and land initial condition for lower atmospheric temperature and winds, land soil temperature, and synoptic wave pattern in the two models. In the next section, we will present the impact of the better initial conditions on reproducing the springtime TP LST/SUBT anomaly and characterizing the summertime precipitation response in the two models.

3.2 The impact on precipitation response to TP LST/SUBT anomaly

In this section, EXP1 and EXP2 with and without nudging initial conditions are used. As described in Sect. 2.2, the pair of 2-month standard experiments (EXP1 and EXP2) is used to quantify the impact of the imposed May TP soil temperature anomaly (land mask) on the June precipitation prediction.

Comparing to the observation, E3SMv1 generally has a cold bias and CIESM has a warm bias over the TP (Fig. 6). This indicates that the imposed land mask will reduce E3SMv1 cold bias and CIESM warm bias to make them warmer and colder, respectively, as shown in Fig. 6. The temperature bias is -0.65 K for EXP1-NudgIC of E3SMv1, − 2.73 K for EXP1 of E3SMv1, 1.36 K for EXP1-NudgIC of CIESM, and 1.80 K for EXP1 of CIESM. The LS4P objective is to examine whether the observed cold May 2003 TP anomaly causes the observed remote June precipitation anomalies over hotspots worldwide. Therefore, EXP1 (cold TP surface) -EXP2 (warm TP surface) for E3SMv1 and EXP2 (cold TP surface) -EXP1 (warm TP surface) for CIESM are used to examine the effect of cold May 2003 anomaly on the global June precipitation anomaly. The May temperature response over the East Asia due to the imposed soil temperature anomalies is shown in Fig. 7. Indeed, the imposed TP soil temperature anomalies are able to produce a cooling effect in all experiments (Fig. 7b–d) as indicated in the observation (Fig. 7a). The spatial map of June precipitation responses and eight hotspots are shown in Figure S3.

We summarize the May 2-m air temperature and June precipitation responses in Fig. 8 and Table S1. All four experiments capture the TP cooling, but the absolute magnitudes are smaller (ranging from − 0.22 to − 0.78 K) than that in the observation (− 1.82 K). Simulations with nudged initial conditions better capture the precipitation responses as observed (Fig. 8b, c). For example, simulations with nudged IC capture the drying over the Northwest America and the wetting over the Southern Great Plains, while simulations without nudged IC produce the opposite signals. Overall, the mean RMSE of precipitation over all eight hot spots are reduced in simulations with nudged initial conditions (1.58 mm/day for E3SMv1 vs 1.06 mm/day for E3SMv1 + NudgIC, and 1.50 mm/day for CIESM and 1.30 mm/day for CIESM + NudgIC).

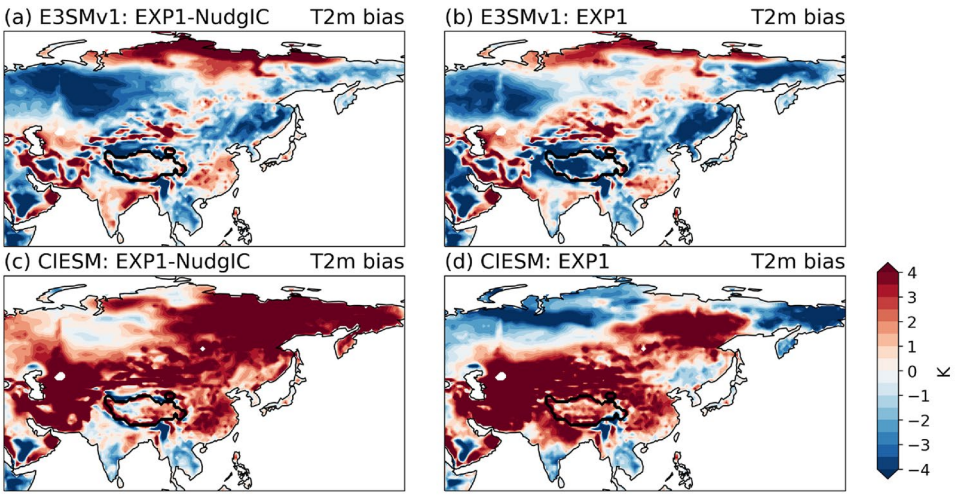

Fig. 6 The simulated May 2-m air temperature (T2m; K) bias relative to observation over East Asia from **a** E3SMv1 EXP1-NudgIC; **b** E3SMv1 EXP1; **c** CIESM EXP1-NudgIC; and **d** CIESM EXP1

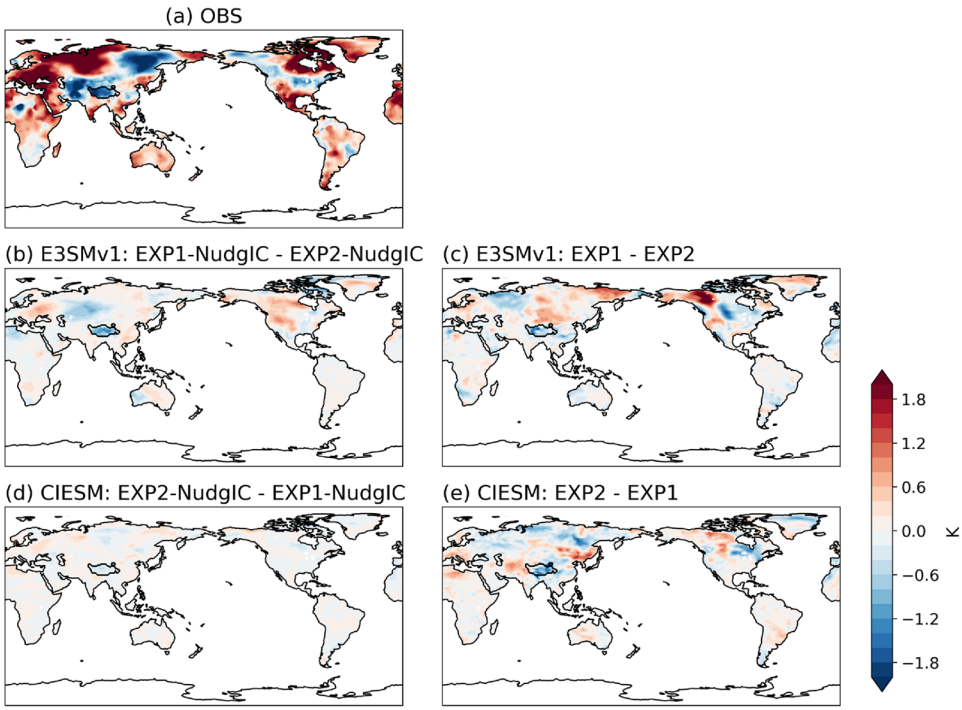

Fig. 7 The 1st–15th May 2003 2-m air temperature (K) anomaly relative to the climatology from observation (**a**) and response due to imposed land mask for E3SMv1 (**b**, **c**) and CIESM (**d**, **e**) with (**b**, **d**) and without (**c**, **e**) nudging ICs

Compared to simulations without nudged ICs, the produced TP 2-m air temperature anomalies are comparable (E3SMv1) or even larger (CIESM) in simulations without nudged ICs (Fig. 8a). However, the June precipitation responses do not align more closely with the observation in those simulations without nudged ICs (Fig. 8b, c). This implies that, besides the ability to reproduce the cooling temperature anomaly as in the observation, the better initial condition, especially the large-scale wave train, is important to reproduce the observational June precipitation responses.

Interestingly, regarding the CIESM model, even if the nudged initial condition is used, the signals of precipitation anomaly are wrong for areas like SYRB, NEastAsia and NW_US. In contrast, E3SMv1 only produces the wrong signal for NEastAsia when using the nudged initial conditions. These model differences are likely related to the different model physics as listed in Table 1. Meanwhile, after using the nudged initial conditions, E3SMv1 better maintains the May temperature anomaly than CIESM. CIESM without the nudged initial conditions produces a comparable temperature anomaly as the observation. It might be caused by the altered land-air interaction after the nudging in CIESM, which makes heat more difficult to be preserved in the soil. Further investigation and sensitivity analysis are required

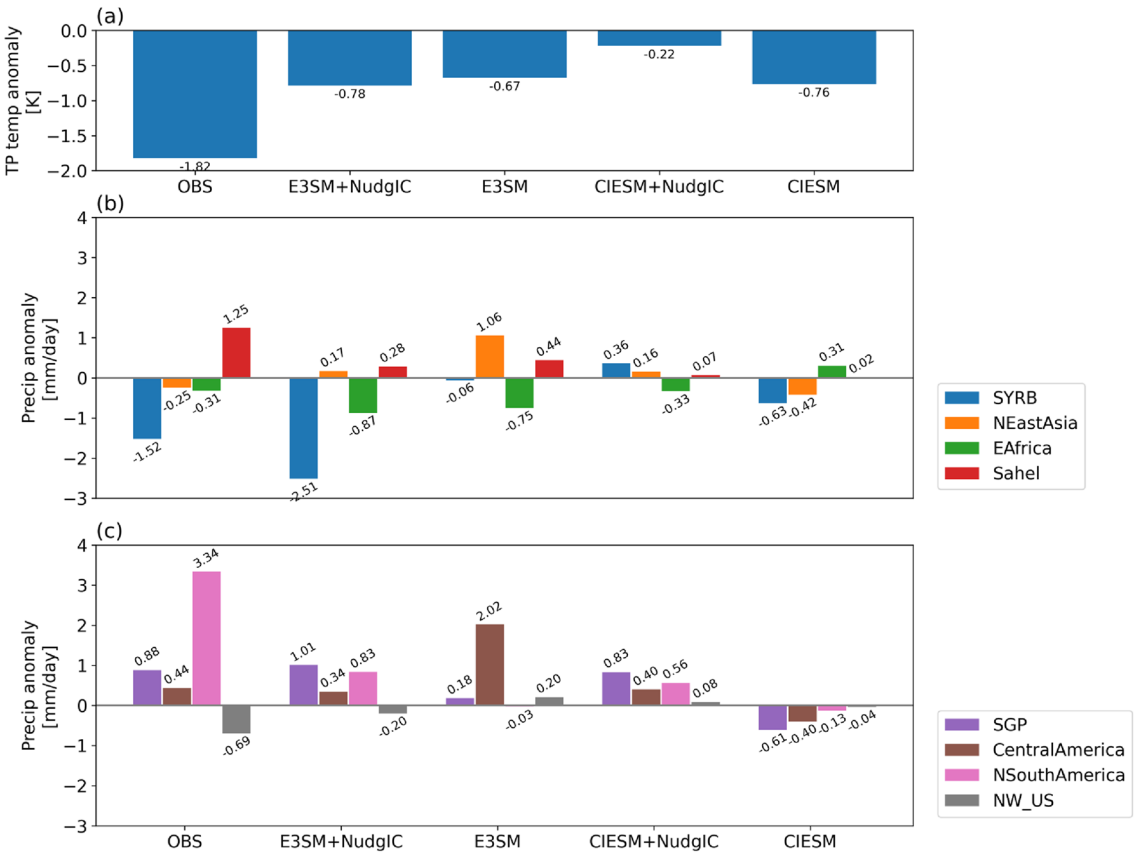

Fig. 8 **a** TP 2-m air temperature anomaly (K) from 1st–15th May 2003 observation, 15-day averaged 2-m air temperature responses in E3SM and CIESM simulations with nudging ICs (i.e., EXP2-NudgIC minus EXP1-NudgIC) and E3SM and CIESM simulations without nudging ICs (i.e., EXP2 minus EXP1) simulations. **b**, **c** June precipitation response (mm/day) over eight hot spots. SYRB: South of Yangtze River Basin (112–121° E; 24–30° N); NEast Asia: North of East Asia (120–135° E; 40–50° N); E Africa: East Africa (27–37° E; 3°S–8° N); Sahel: Sahel (12° W–13° E; 10.5–16° N); SGP: Southern Great Plains (105–90° W; 30–40° N); Central America: Central America (110–87° W; 13–29.5° N); N South America: Northern South America (80–51° W; 4–12.5° N); and NW_US: Northwest United States (124–105° W; 45–55° N). The definitions of hotspots are referred from Xue et al. (2022)

to comprehensively understand the specific reasons behind the model discrepancy but beyond the scope of this study.

4 Conclusions and discussions

Our study demonstrates the importance of the nudging approach to produce a more realistic initial condition to investigate the impact of LST/SUBT anomaly on subseasonal-to-seasonal (S2S) precipitation prediction with two climate models. Nudging towards the reanalysis winds, the model initial conditions (of both atmosphere and land) become more consistent with observations. Furthermore, using the nudged initial conditions lead to a more consistent June precipitation responses to the imposed TP LST/SUBT anomaly globally while compared with the observation. Overall, our findings emphasize the important role that more realistic initial conditions, especially the large-scale wave train, play when applying climate models for S2S prediction in the context of mimicking observations for selected time periods.

The May temperature can quickly deviate from the nudged initial conditions when models begin to freely run in May 2003 due to the short memory of the atmosphere. However, simulations with nudged initial conditions better capture the June precipitation responses worldwide. This likely manifests the combined effect of the imposed soil temperature anomaly, more reasonable initial conditions (including large-scale circulation patterns) and slightly better soil temperature profile (then soil memory), which can help regulate the large-scale circulation and the responsive wave train that affect the remote S2S precipitation responses. Although the simulated soil temperature profiles with nudging are slightly better in some observation sites, they still have large biases compared with the observation. Unfortunately, both models lack the nudging capability in their current land models. When such a capability becomes available in future versions, we expect that applying the

nudging approach to the land component might be helpful to improve initial conditions of the land model and further improve the S2S precipitation predictions.

Some experiments produce a weaker May 2-m air temperature anomaly relative to the observation, partly because the model's inability to maintain the cold temperature anomaly for the entire month. This inability to maintain the cold temperature anomaly for the whole month may be the cause of the weak precipitation response over the upstream regions, like Sahel. Previous studies indicated that the upstream precipitation response is linked to the zonal and meridional circulation anomalies due to the anomalous Tibetan heating or cooling (Lu et al. 2018; Nan et al. 2019), rather than the downstream TRC wave train (Xue et al. 2022).

In this study, we find that good initial conditions are critical in successfully simulating the impact of LST/SUBT on precipitation predictability for climate models. However, as shown in Fig. 8, the two models still have significant discrepancies in capturing the precipitation, especially over hot spots in East Asia. This hints that the climate model's skill to capture near downstream relationships may also require more reasonable representations of the complex topography and better initialized land components, which can be achieved by high-resolution models, such as the high-resolution E3SMv1 (Caldwell et al. 2019) and the regionally refined E3SM configurations (Tang et al. 2019, 2023). It would be helpful to further explore the impact of different resolutions on S2S prediction, and evaluate their contributions compared to the better initial condition as shown in this study. Considering the high computational cost of the globally uniform high-resolution model, regional refined models (e.g., Tang et al. 2019; 2023) provide good opportunities to explore the model resolution impacts on S2S prediction in an economic way. Recent studies (Hoffmann et al. 2019; Hersbach et al. 2020) show that ERA5 performs better than ERA-Interim when used in a nudging simulation, especially for near-surface fields and precipitation. Incorporating ERA5 in the ongoing LS4P Phase II could help expand on the findings of the current study and perform a robust cross-validation of results obtained from ERA-Interim. Furthermore, soil moisture is also important to generate a realistic initial condition for S2S prediction (Ardilouze and Boone 2023). Its impacts deserve further investigations in further LS4P activities.

Supplementary Information The online version contains supplementary material available at https://doi.org/10.1007/s00382-023-07082-1.

Author contributions YQ processed the simulations, carried out all calculations and wrote the main manuscript text. QT designed the paper scope and structure and revised the paper. YKX, YL and YLL provided the main observation data and help in polishing this paper and offered constructive comments.

Funding This research was supported by the Energy Exascale Earth System Model (E3SM) project, funded by the U.S. Department of Energy (DOE), Office of Science, Office of Biological and Environmental Research (BER), and National Science Foundation AGS-1849654. Support has been received from the Lawrence Livermore National Laboratory (LLNL) LDRD projects 22-ERD-008, "Multi-scale Wildfire Simulation Framework and Remote Sensing". LLNL is operated by Lawrence Livermore National Security, LLC, for the U.S. DOE, National Nuclear Security Administration under Contract DE-AC52-07NA27344. The Pacific Northwest National Laboratory (PNNL) is operated for the DOE by the Battelle Memorial Institute under Contract DE-AC05-76RL01830.

Data availability The simulations with nudging initial conditions are accessed from the National Tibetan Plateau Data Center (http://data.tpdc.ac.cn/en/). The evaluation data sets are from https://doi.org/10.5281/zenodo.4383284 (Xue and Diallo, 2021). The ERA-interim reanalysis datasets are downloaded from https://apps.ecmwf.int/archive-catalogue/?class=ei.

Declarations

Conflict of interest The authors have no relevant financial or non-financial interests to disclose.

References

Ardilouze C, Boone AA (2023) Impact of accounting for a thermally-balanced soil state on subseasonal predictability. Res Sq. https://doi.org/10.21203/rs.3.rs-3167226/v1

Arias P, Bellouin N, Coppola E et al (2021) Climate change 2021: the physical science basis. Contribution of Working Group I to the Sixth Assessment Report of the Intergovernmental Panel on Climate Change; Technical Summary

Beljaars ACM, Brown AR, Wood N (2004) A new parametrization of turbulent orographic form drag. Q J R Meteorol Soc 130:1327–1347. https://doi.org/10.1256/qj.03.73

Boyle JS, Williamson D, Cederwall R et al (2005) Diagnosis of community atmospheric model 2 (CAM2) in numerical weather forecast configuration at atmospheric radiation measurement sites. J Geophys Res Atmos. https://doi.org/10.1029/2004JD005042

Bretherton CS, Park S (2009) A new moist turbulence parameterization in the community atmosphere model. J Clim 22:3422–3448. https://doi.org/10.1175/2008JCLI2556.1

Caldwell PM, Mametjanov A, Tang Q et al (2019) The DOE E3SM coupled model version 1: description and results at high resolution. J Adv Model Earth Syst 11:4095–4146. https://doi.org/10.1029/2019MS001870

Craig AP, Vertenstein M, Jacob R (2012) A new flexible coupler for earth system modeling developed for CCSM4 and CESM1. Int J High Perform Comput Appl 26:31–42. https://doi.org/10.1177/1094342011428141

Dee DP, Uppala SM, Simmons AJ et al (2011) The ERA-Interim reanalysis: configuration and performance of the data assimilation system. Q J R Meteorol Soc 137:553–597. https://doi.org/10.1002/qj.828

Dennis JM, Edwards J, Evans KJ et al (2012) CAM-SE: a scalable spectral element dynamical core for the community atmosphere model. Int J High Perform Comput Appl 26:74–89

Eyring V, Bony S, Meehl GA et al (2016) Overview of the coupled model intercomparison project phase 6 (CMIP6) experimental design and organization. Geosci Model Dev 9:1937–1958. https://doi.org/10.5194/gmd-9-1937-2016

Gao L, Bernhardt M, Schulz K, Chen X (2017) Elevation correction of ERA-Interim temperature data in the Tibetan Plateau: TEMPERATURE CORRECTION IN THE TIBETAN PLATEAU. Int J Climatol 37:3540–3552. https://doi.org/10.1002/joc.4935

Gates WL, Boyle JS, Covey C et al (1999) An overview of the results of the atmospheric model intercomparison project (AMIP I). Bull Am Meteorol Soc 80:29–56. https://doi.org/10.1175/1520-0477(1999)080%3c0029:AOOTRO%3e2.0.CO;2

Gettelman A, Morrison H (2015) Advanced two-moment bulk microphysics for global models. Part I: off-line tests and comparison with other schemes. J Clim 28:1268–1287. https://doi.org/10.1175/JCLI-D-14-00102.1

Golaz J-C, Larson VE, Cotton WR (2002) A PDF-based model for boundary layer clouds. Part I: method and model description. J Atmos Sci 59:3540–3551. https://doi.org/10.1175/1520-0469(2002)059%3c3540:APBMFB%3e2.0.CO;2

Golaz J, Caldwell PM, Van Roekel LP et al (2019) The DOE E3SM coupled model version 1: overview and evaluation at standard resolution. J Adv Model Earth Syst 11:2089–2129. https://doi.org/10.1029/2018MS001603

Hersbach H, Bell B, Berrisford P et al (2020) The ERA5 global reanalysis. Q J R Meteorol Soc 146:1999–2049. https://doi.org/10.1002/qj.3803

Hoffmann L, Günther G, Li D et al (2019) From ERA-interim to ERA5: the considerable impact of ECMWF's next-generation reanalysis on Lagrangian transport simulations. Atmos Chem Phys 19:3097–3124. https://doi.org/10.5194/acp-19-3097-2019

Huang H, Xue Y, Chilukoti N et al (2020) Assessing global and regional effects of reconstructed land-use and land-cover change on climate since 1950 using a coupled land–atmosphere–ocean model. J Clim 33:8997–9013. https://doi.org/10.1175/JCLI-D-20-0108.1

Iacono MJ, Delamere JS, Mlawer EJ et al (2008) Radiative forcing by long-lived greenhouse gases: calculations with the AER radiative transfer models. J Geophys Res 113:D13103. https://doi.org/10.1029/2008JD009944

Jeuken ABM, Siegmund PC, Heijboer LC et al (1996) On the potential of assimilating meteorological analyses in a global climate model for the purpose of model validation. J Geophys Res Atmos 101:16939–16950. https://doi.org/10.1029/96JD01218

Kooperman GJ, Pritchard MS, Ghan SJ et al (2012) Constraining the influence of natural variability to improve estimates of global aerosol indirect effects in a nudged version of the community atmosphere model 5. J Geophys Res Atmos. https://doi.org/10.1029/2012JD018588

Larson VE, Golaz J-C (2005) Using probability density functions to derive consistent closure relationships among higher-order moments. Mon Weather Rev 133:1023–1042. https://doi.org/10.1175/MWR2902.1

Larson J, Jacob R, Ong E (2005) The model coupling toolkit: a new fortran90 toolkit for building multiphysics parallel coupled models. Int J High Perform Comput Appl 19:277–292. https://doi.org/10.1177/1094342005056115

Liang Y, Wang L, Zhang GJ, Wu Q (2017) Sensitivity test of parameterizations of subgrid-scale orographic form drag in the NCAR CESM1. Clim Dyn 48:3365–3379. https://doi.org/10.1007/s00382-016-3272-7

Lin Y, Huang X, Liang Y et al (2020) Community integrated earth system model (CIESM): description and evaluation. J Adv Model Earth Syst. https://doi.org/10.1029/2019MS002036

Liu X, Ma P-L, Wang H et al (2016) Description and evaluation of a new four-mode version of the modal aerosol module (MAM4) within version 5.3 of the community atmosphere model. Geosci Model Dev 9:505–522. https://doi.org/10.5194/gmd-9-505-2016

Liu L, Zhang C, Li R et al (2018) C-Coupler2: a flexible and user-friendly community coupler for model coupling and nesting. Geosci Model Dev 11:3557–3586. https://doi.org/10.5194/gmd-11-3557-2018

Lu M, Yang S, Li Z et al (2018) Possible effect of the Tibetan Plateau on the "upstream" climate over West Asia, North Africa, South Europe and the North Atlantic. Clim Dyn 51:1485–1498. https://doi.org/10.1007/s00382-017-3966-5

Ma H-Y, Chuang CC, Klein SA et al (2015) An improved hindcast approach for evaluation and diagnosis of physical processes in global climate models: AN IMPROVED HINDCAST APPROACH. J Adv Model Earth Syst 7:1810–1827. https://doi.org/10.1002/2015MS000490

Mariotti A, Ruti PM, Rixen M (2018) Progress in subseasonal to seasonal prediction through a joint weather and climate community effort. Npj Clim Atmos Sci 1:4. https://doi.org/10.1038/s41612-018-0014-z

Merryfield WJ, Baehr J, Batté L et al (2020) Current and emerging developments in subseasonal to decadal prediction. Bull Am Meteorol Soc 101:E869–E896. https://doi.org/10.1175/BAMS-D-19-0037.1

Morrison H, Gettelman A (2008) A new two-moment bulk stratiform cloud microphysics scheme in the community atmosphere model, version 3 (CAM3). Part I: description and numerical tests. J Clim 21:3642–3659. https://doi.org/10.1175/2008JCLI2105.1

Nan S, Zhao P, Chen J (2019) Variability of summertime Tibetan tropospheric temperature and associated precipitation anomalies over the central-eastern Sahel. Clim Dyn 52:1819–1835. https://doi.org/10.1007/s00382-018-4246-8

Neale R, Chen C, Gettelman A et al (2012) Description of the community atmosphere model (CAM5) NCAR tech note NCAR. TN-486 STR

Oleson W, Lawrence M, Bonan B, et al (2010) Technical description of version 4.0 of the community land model (CLM). https://doi.org/10.5065/D6FB50WZ

Park S, Bretherton CS (2009) The University of Washington shallow convection and moist turbulence schemes and their impact on climate simulations with the community atmosphere model. J Clim 22:3449–3469. https://doi.org/10.1175/2008JCLI2557.1

Phillips TJ, Potter GL, Williamson DL et al (2004) Evaluating parameterizations in general circulation models: climate simulation meets weather prediction. Bull Am Meteorol Soc 85:1903–1916. https://doi.org/10.1175/BAMS-85-12-1903

Qin Y, Lin Y, Xu S et al (2018) A diagnostic PDF cloud scheme to improve subtropical low clouds in NCAR community atmosphere model (CAM 5). J Adv Model Earth Syst 10:320–341. https://doi.org/10.1002/2017MS001095

Rasch PJ, Xie S, Ma P-L et al (2019) An overview of the atmospheric component of the energy exascale earth system model. J Adv Model Earth Syst 11:2377–2411. https://doi.org/10.1029/2019MS001629

Seller PJ (1985) Canopy reflectance, photosynthesis and transpiration. Int J Remote Sens 6:1335–1372. https://doi.org/10.1080/01431168508948283

Song X, Zhang GJ (2011) Microphysics parameterization for convective clouds in a global climate model: description and single-column model tests. J Geophys Res 116:D02201. https://doi.org/10.1029/2010JD014833

Stevens B, Fiedler S, Kinne S et al (2017) MACv2-SP: a parameterization of anthropogenic aerosol optical properties and an associated Twomey effect for use in CMIP6. Geosci Model Dev 10:433–452. https://doi.org/10.5194/gmd-10-433-2017

Sun J, Zhang K, Wan H et al (2019) Impact of nudging strategy on the climate representativeness and Hindcast skill of constrained EAMv1 simulations. J Adv Model Earth Syst 11:3911–3933. https://doi.org/10.1029/2019MS001831

Tang Q, Klein SA, Xie S et al (2019) Regionally refined test bed in E3SM atmosphere model version 1 (EAMv1) and applications for high-resolution modeling. Geosci Model Dev 12:2679–2706. https://doi.org/10.5194/gmd-12-2679-2019

Tang Q, Golaz J-C, Van Roekel LP et al (2023) The fully coupled regionally refined model of E3SM version 2: overview of the atmosphere, land, and river results. Geosci Model Dev 16:3953–3995. https://doi.org/10.5194/gmd-16-3953-2023

Verhoef A, Bruin HARD, Hurk BJJMVD (1997) Some practical notes on the parameter kB−1 for sparse vegetation. J Appl Meteorol Climatol 36:560–572. https://doi.org/10.1175/1520-0450(1997)036%3c0560:SPNOTP%3e2.0.CO;2

Wang Y, Zhang GJ, Craig GC (2016) Stochastic convective parameterization improving the simulation of tropical precipitation variability in the NCAR CAM5: STOCHASTIC CONVECTIVE PARAMETERIZATION. Geophys Res Lett 43:6612–6619. https://doi.org/10.1002/2016GL069818

Xie S, Ma H-Y, Boyle JS et al (2012) On the correspondence between short- and long-time-scale systematic errors in CAM4/CAM5 for the year of tropical convection. J Clim 25:7937–7955. https://doi.org/10.1175/JCLI-D-12-00134.1

Xue Y, Diallo I (2020) LS4P-I evaluation datasets for the paper organization and experimental design

Xue Y, Fennessy MJ, Sellers PJ (1996) Impact of vegetation properties on US summer weather prediction. J Geophys Res Atmos 101:7419–7430. https://doi.org/10.1029/95JD02169

Xue Y, Yao T, Boone AA et al (2021) Impact of initialized land surface temperature and snowpack on subseasonal to seasonal prediction project, phase I (LS4P-I): organization and experimental design. Geosci Model Dev 14:4465–4494. https://doi.org/10.5194/gmd-14-4465-2021

Xue Y, Diallo I, Boone AA et al (2022) Spring land temperature in tibetan plateau and global-scale summer precipitation: initialization and improved prediction. Bull Am Meteorol Soc 103:E2756–E2767. https://doi.org/10.1175/BAMS-D-21-0270.1

Zhang F, Li J (2013) Doubling-adding method for delta-four-stream spherical harmonic expansion approximation in radiative transfer parameterization. J Atmospheric Sci 70:3084–3101. https://doi.org/10.1175/JAS-D-12-0334.1

Zhang GJ, McFarlane NA (1995) Sensitivity of climate simulations to the parameterization of cumulus convection in the Canadian climate centre general circulation model. Atmos Ocean 33:407–446. https://doi.org/10.1080/07055900.1995.9649539

Zhang K, Wan H, Liu X et al (2014) Technical Note: On the use of nudging for aerosol–climate model intercomparison studies. Atmos Chem Phys 14:8631–8645. https://doi.org/10.5194/acp-14-8631-2014

Zhao X, Lin Y, Peng Y et al (2017) A single ice approach using varying ice particle properties in global climate model microphysics. J Adv Model Earth Syst 9:2138–2157. https://doi.org/10.1002/2017MS000952